

## Dynamics of electro-optical switching in the antiferroelectric $B_2$ phase of an achiral bent-core shape compound

Lev M. Blinov and Mikhail I. Barnik

*Institute of Crystallography, Russian Academy of Science, Leninsky prosp.59, Moscow, 117333, Russia*

E. Soto Bustamante

*University of Chile, Olivos, Santiago, Chile*

Gerhard Pelzl and Wolfgang Weissflog

*Institute of Physical Chemistry, MLU Halle-Wittenberg, Mühlpforte 1, 06108 Halle (S), Germany*

(Received 16 April 2002; published 26 February 2003)

A detailed study of the dynamics of electro-optical response has been carried out over the whole temperature range of the antiferroelectric  $B_2$  phase of a compound with bent-core shape molecules, a homolog ( $n=14$ ) of the series 4-chloro-1,3-phenylene bis[4-(4- $n$ -alkylphenylimino)benzoates]. Two types of stripe domains were observed with opposite handedness and simultaneous clock and anticlock motion of the director in the neighboring domains. The temperature dependence of the interlayer potential has been found from the threshold of the transition from the ground antiferroelectric (AF) state to the field-induced ferroelectric (F) state. The rotational viscosity  $\gamma_\varphi$  has been calculated from the dynamics of the field-induced azimuthal director switching between F-F and AF-F states and free relaxation of the director from F to AF state. The electro-optical response was also observed below the AF-F threshold. The latter was attributed to the soft-mode distortion of the molecular tilt angle in the vicinity of the transition from the  $B_2$  phase to the isotropic phase.

DOI: 10.1103/PhysRevE.67.021706

PACS number(s): 61.30.Cz, 61.30.Gd, 42.79.Kr

### I. INTRODUCTION

Recently liquid crystalline polar [1], antiferroelectric [2–4], and ferroelectric [5] compounds have been designed which, in contrast to well known liquid crystalline ferroelectric (FLC) and antiferroelectric (AFLC) liquid crystals [6,7], are composed of achiral molecules and show high magnitude of the electric polarization (see for review, Ref. [8]). New compounds consisting of bent-core (or banana-) shape molecules [2,4,5] form many different phases, among them the  $B_2$  phase seems to be the most interesting from the fundamental point of view. Due to spontaneous breaking of symmetry, the achiral medium forms two types of chiral domains [9], left (HL) and right (HR) in equal proportion, and also racemic domains ( $R$ ). The ground, zero-field state of the  $R$  domains is synclinic (molecules are tilted with the same azimuthal angle) but with the opposite direction of the in-plane polarization in the neighboring layers. Under an electric field exceeding a certain threshold, the polarization follows the field direction and the structure becomes anticlinic with the opposite tilt in the neighboring layers and uniform polarization. The ground state of the HL and HR states is anticlinic (but also with alternating direction of the local polarization) and the field-induced state is synclinic, like in the (smectic) Sm-C\* phase, with uniform macroscopic polarization along the field direction.

Needless to say that dynamics of bent-shape compound switching is even more complicated than that of the FLC and AFLC. However, even for conventional, chiral AFLC the experimental data on the subject are very rare. In fact, their dynamics was studied both theoretically [7] and experimentally (see, e.g., [10,11]) mostly in the low-field limit. We were able to find only few papers on AFLC, e.g., [12,13], in

which high-field relaxation times and rotational viscosity have been measured for chiral AFLC compounds. As to achiral bent-core compounds, up to now, only qualitative results on kinetics of the polarization reversal [14–16] and field-induced texture changes [17] are available. For instance, according to our knowledge, a quantitative estimate of the rotational viscosity has been made only in one paper [18].

The aim of the present paper is to investigate the dynamics of the director switching for a bent-core compound that has the  $B_2$  phase at relatively low temperature and reveals very high value of spontaneous polarization [16,19]. In this work, the director dynamics was studied over the whole temperature range of the  $B_2$  phase in different regimes, below and above the field-induced ferroelectric-antiferroelectric transition. In the compound studied, as a result of symmetry breaking, two systems of chiral stripe domains form, each behaving as a conventional chiral ferroelectric. The latter allows for a quantitative interpretation of experimental data using a theoretical approach developed for chiral AFLC [20]. Therefore, in Sec. II, we briefly remind a theoretical background developed for chiral AFLC, which is used later on for interpretation of experimental data. In Sec. III, the results on electro-optical switching and a threshold for the field-induced transition between the ground ferroelectric and field-induced antiferroelectric states are discussed. Finally, in Sec. IV the temperature and field dependencies of the electro-optical switching times are presented and the rotational viscosity and relevant elastic properties of the compound are discussed.

### II. BACKGROUND

We would like to discuss our achiral antiferroelectric in terms of a conglomerate of two subsystems (or domains) of

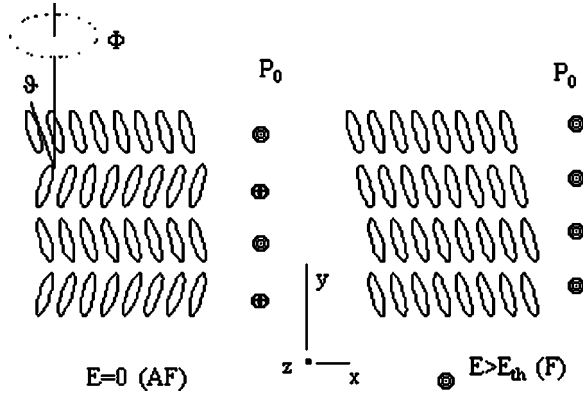


FIG. 1. A structure of a chiral antiferroelectric liquid crystal below (left) and above (right) the field-induced AF-F transition.

conventional chiral AFLC of opposite handedness. We shall ignore the difference between racemic and chiral domains because they behave quite similarly in dynamic experiments [16,18].

In Fig. 1 (left) a model of a chiral (but helix free) AFLC is presented. Molecules form a lamellar smectic phase with a normal along the rubbing direction  $y$  and with alternating tilt of the same amplitude  $\pm\vartheta$  and phase  $\Phi$  differing by  $\pi$  in the neighboring layers. The electric field is supposed to be applied in the smectic layer plane along the  $z$  axis. Due to chirality each layer possesses polarization  $P_0$  perpendicular to the tilt plane. The total polarization in the ground state is zero and the antiferroelectric Sm- $C_A$  phase is nonpolar. With increasing external field a transition is observed from the antiferroelectric (AF) ground state to the ferroelectric (F) field-induced state, Fig. 1 (right). After transition, all  $P_0$  are oriented along the field and the director azimuth is the same in all smectic layers,  $\Phi=0$ . Such a transition in conventional chiral AFLC is of first order and begins with nucleation of solitary orientational waves [20,21].

The behavior of infinite AFLC samples below the AF-F threshold is carefully analyzed in Ref. [7]. In dynamics of the two-component order parameter, four different modes [or four branches of the dispersion curves,  $\tau^{-1}(q)$ ] have been found, two antiferroelectric (amplitude  $\vartheta$  and phase  $\varphi$  of the tilt) and two ferroelectric. The antiferroelectric branches for AFLC with helical wave vector  $q_a$  have the following structure:

$$\begin{aligned}\tau_{\vartheta}^{-1}(AF) &= \frac{2\alpha}{\gamma}(T_a - T) + \frac{K_a}{\gamma}(q \pm q_a)^2, \\ \tau_{\varphi}^{-1}(AF) &= \frac{K_a}{\gamma}(q \pm q_a). \end{aligned} \quad (1)$$

Here,  $T_a$  is temperature of transition from Sm-A to Sm- $C_A$  phase,  $K_a$  is nematiclike elastic modulus, and  $\alpha_0$  is Landau coefficient. The viscosity coefficient  $\gamma$  is taken for both modes. Note that for excitations with wave vector  $q = q_a$ , for example, in light scattering experiments,  $(\tau_{\varphi})^{-1}$  is zero at any temperature (gapless Goldstone mode, called also acoustic branch) and  $(\tau_{\vartheta})^{-1}$  tends to zero at  $T_a$  (antiferro-

electric soft mode). In uniform electric field,  $q=0$ , the softening is somewhat incomplete.

The structure of ferroelectric  $(\tau_{\varphi})^{-1}(F)$  and  $(\tau_{\vartheta})^{-1}(F)$  branches is more complicated, however, both of them include terms of  $(\alpha_0/\gamma)(T - T_f)$  type, where  $T_f$  is a virtual temperature of transition to a ferroelectric phase (which may even not exist). Therefore, the mode softening at  $T_a$  is far to be complete due to term  $(T_a - T_f)$ . Nevertheless, a lower frequency ferroelectric  $\varphi$  mode (called also optical branch) was observed in the experiments [7].

The field-induced azimuthal motion of the director below and above the AF-F threshold has been discussed theoretically in Refs. [20,21]. For finite size samples, the distortions below the AF-F threshold remind the Frederiks transition in nematics. The density of the bulk free energy in the simplest case [21] was taken in the form

$$\begin{aligned} F = \frac{1}{2} K \left[ \left( \frac{\partial \Phi_i}{\partial x} \right)^2 + \left( \frac{\partial \Phi_i}{\partial z} \right)^2 \right] + W \cos(\Phi_{i+1} - \Phi_i) \\ - P_0 E \cos \Phi_i. \end{aligned} \quad (2)$$

Here, the first term describes the nematiclike elastic energy in one constant approximation ( $K \approx K_N \sin^2 \vartheta$ ). All specific properties of an AFLC are included in the second term of Eq. (2), which corresponds solely to interaction between molecules in the neighboring layers. Moreover, only the first harmonic of interlayer potential  $W$  is taken into consideration (a role of the second harmonic is discussed in Ref. [20]). The third term describes interaction of the external field  $E$  with the layer polarization. Although for substances with high  $P_0$  the dielectric anisotropy can be neglected, the quadratic-in-field effects are still taken into account by terms proportional to  $P^2$ .

The solution of Eq. (2) depends on further simplifications. If one assumes that the director in the odd layers with  $\Phi_i = 0$  is unaffected by an external field and only the azimuth in the even layers  $\Phi_{i+1}$  is changed from  $\pi$  to 0, then, for infinitely thick sample ( $z \rightarrow \infty$ ), the torque balance equation reduces to the form

$$\gamma_{\varphi} \frac{\partial \Phi}{\partial t} = K \frac{\partial^2 \Phi}{\partial x^2} + (2W - P_0 E) \sin \Phi. \quad (3)$$

Here, to describe the dynamics of  $\Phi$  at constant  $\vartheta$ , the viscous torque is introduced with viscosity coefficient  $\gamma_{\varphi} = \gamma \sin^2 \vartheta$  [22]. If the elastic term is discarded and  $\sin \Phi \rightarrow \Phi$ , Eq. (3) would predict a second-order field-induced AF-F transition with a threshold field for the distortion

$$E_{th} = \frac{2W}{P_0}, \quad (4)$$

and the following inverse switching times for the AF-F transition and back relaxation ( $E=0$ ) from the F to the AF state

$$\tau_{AF}^{-1} = \frac{1}{\gamma_{\varphi}} (P_0 E - 2W), \quad (5)$$

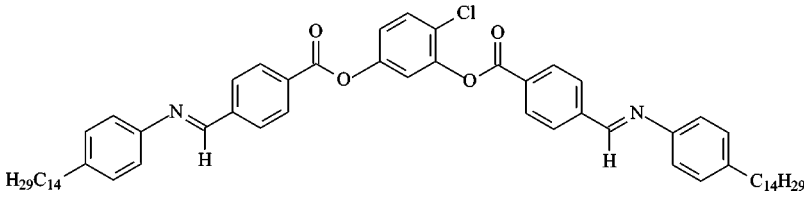


FIG. 2. Structural formula of the investigated compound.

$$\tau_{FA}^{-1} = \frac{2W}{\gamma_{\varphi}}. \quad (6)$$

In reality the AF-F transition is of first order and it can be described in terms of two variable angles  $\delta = (\psi - \varphi)/2$  and  $\beta = (\psi + \varphi)/2$  where, in accordance with Eq. (2), in odd layers  $\Phi_i = \varphi$  and in even layers  $\Phi_{i+1} = \pi - \psi$  with  $\varphi = \psi = 0$  in the ground state [20]. Close to the field-induced AF-F transition, angle  $\beta$  is saturated at  $\pi/2$  and the transition is controlled solely by an angle  $\alpha$ . With a contribution of the second-harmonic amplitude in the interlayer potential  $J$  varied numerically in the range  $(0.1-0.5)W$ , the threshold field was found to be

$$E_{A-F} = \frac{(3.2-2.4)W}{P_0}. \quad (7)$$

At low fields much below  $E_{A-F}$ , angle  $\alpha$  is small and the whole situation is controlled by angle  $\beta$ . For samples of a finite thickness  $d$  and infinite anchoring energy, the theory predicts the Frederiks transition with a voltage threshold  $U_{th} = (2\pi/P_0)(WK)^{1/2}$ . Above the Frederiks threshold (but still below the AF-F threshold) the relaxation rate of the  $\beta$  distortion is quadratic-in-field and follows the expression [23]:

$$\tau_a^{-1} = \frac{1}{2\gamma_{\varphi}} \left( \frac{P_0^2 E^2}{4W} + Kq_i^2 \right). \quad (8)$$

In geometry of Fig. 1,  $q_i$  is a wave vector of any distortion along the  $z$  or  $x$  coordinates.

### III. EXPERIMENT

#### A. Material and cells

The substance studied is an alkyl homologue ( $n=14$ ) of the series 4-chloro-1,3-phenylene bis[4-(4- $n$ -alkylphenylimino)benzoates] Fig. 2 investigated earlier [16,19]. It is crystalline at room temperature, and has the  $B_2$  antiferroelectric phase in the range 70–127 °C. The first-order transition to the isotropic phase with a temperature hysteresis in the range 123–128 °C is accompanied by large enthalpy of 14.9 kJ/mol. The dependence of polarization on the applied voltage manifests a hysteresis typical of the AFLCs, with the maximum field switched polarization  $P_{sw,max} = P_0 = 380$  nC/cm<sup>2</sup>, almost independent of temperature [16].

The cells were made of two indium-tin oxide covered glass plates separated by Teflon stripes to form a 10  $\mu$ m gap (measured by capacitance of the empty cells) with an electrode overlapped area about 4×4 mm. Relatively large

thickness was chosen in order to avoid boundary effects. The inner surfaces of the cells were covered by 100-nm-thick polyimide layers (Nissan Chemical Industry RN-1266) and rubbed unidirectionally. The cells were filled with a liquid crystal in the isotropic phase and placed in a sample holder with optical windows providing microscopic observations under temperature control. Figure 1 corresponds to the top view under a microscope with the rubbing direction along the  $y$  axis.

#### B. Technique

In this work, we used three methods for studying the AF-F threshold and dynamics of the director (and polarization) switching:

(1) For measurements of the threshold field for AF-F transition, we applied to a cell a low frequency triangular voltage form (amplitude  $U_m = 100$  V, frequency  $f = 1.3$  Hz) and observe the electro-optical response with a digital oscilloscope. The cell was installed under a microscope with the rubbing direction along the light electric vector and with an analyzer in the crossing position. Filtered light from the microscope was used for cell illumination and the optical transmission could be observed by eye or recorded using a photomultiplier and charge-coupled device camera.

(2) For investigations of dynamics of the director below and above the AF-F transition, we also used electro-optical measurements but with a special shape of voltage form. As expected for two kinds of domains with opposite chirality, the sign of the electro-optical response is the same for pulses of positive and negative polarity and a standard rectangular voltage form with duty ratio  $D = 1$  cannot be used for studying relaxation processes. Therefore, we synthesized polar (positive and negative) pulses with duration 20–30 ms and separated by 100–200 ms interval. In this case, after application of each voltage pulse the liquid crystal has enough time to relax completely. With a digital oscilloscope, we could measure both voltage-on and voltage-off times  $t_{on}$  and  $t_{off}$  at different voltage and temperature.

(3) For studying dynamics of the field-induced F-F transition, a square-wave voltage form ( $U_m = 100$  V,  $f = 50$  Hz) was applied to the cells. In this case, the ground, antiferroelectric state is bypassed and the corresponding switching times  $t_{sw}$  can be different from  $t_{on}$  and  $t_{off}$ . In experiment, we measured both the front of the electro-optical response and the width of the repolarization current pulse, well correlating with each other. However, the criterion for calculation of  $t_{sw}$  from the current response is more precise [6] and the current peak technique was thus preferred.

### IV. RESULTS AND DISCUSSION

#### A. Texture and electro-optical response

As shown earlier [17,18], textures of the  $B_2$  phase are strongly dependent on cell treatment by electric field and

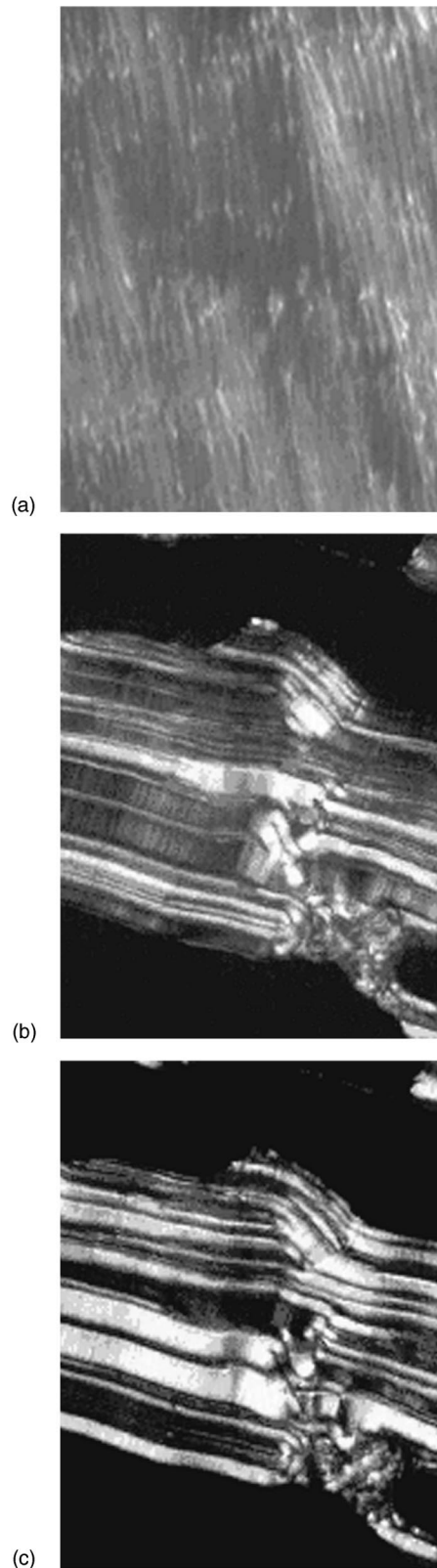


FIG. 3. (a) The initial texture of the  $B_2$  phase (no field, crossed polarizers, rubbing direction is vertical,  $T=80^\circ\text{C}$ , photo size  $0.46 \times 0.34 \text{ mm}^2$ ); (b),(c) Stripe domains of alternating brightness at  $-80 \text{ V}$  (b) and  $+80 \text{ V}$  (c) (a video picture at square-wave field,  $\pm 80 \text{ V}$ , frequency  $2 \text{ Hz}$ ,  $\alpha=15^\circ$ ,  $T=100^\circ\text{C}$ , photo size  $0.46 \times 0.34 \text{ mm}^2$ ).

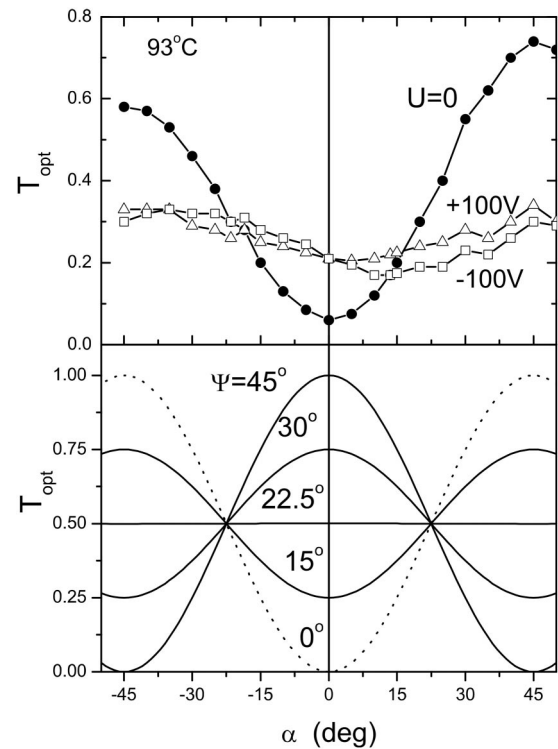


FIG. 4. (a) Optical transmission of a cell as a function of rotation angle of a microscope table for voltages  $U=0$ ,  $+100 \text{ V}$ , and  $-100 \text{ V}$  (polar pulses  $20 \text{ ms}$ , interval  $100 \text{ ms}$ ). Note, that the observed optical response amplitude corresponds to a difference between field-induced and zero-field transmission (positive for  $|\alpha| < 20^\circ$  and negative for  $|\alpha| > 20^\circ$ ). (b) Calculated dependencies of the optical transmission for the two chiral domain systems on table rotation angle  $\alpha$  and field-induced director rotation angle  $\Psi$ .

thermal prehistory. One of our original textures is shown in Fig. 3(a). It has been obtained after filling the cell in the isotropic phase and cooled down to the  $B_2$  phase without field applied. Between crossed polarizers the texture is quite uniform with focal conic domains parallel to the rubbing direction seen on the black background. Under the field applied the texture changes but still shows very small domains with typical size of  $2\text{--}5 \mu\text{m}$ . Such a fine-grain texture shows weak electro-optical response. In our present work, the measurements in the  $B_2$  phase were performed on the coarse-grain textures prepared by the treatment of a sample with the square-wave voltage ( $100 \text{ V}$ ,  $50 \text{ Hz}$ ) on slow cooling from the isotropic phase. Such textures show the electro-optical response one order of magnitude higher than that of the fine-grain textures (the absolute value of the optical transmission reach the level of about 10% with respect to the transmission of an empty cell between parallel polarizers).

The optical transmission was measured using a light spot of diameter about  $400 \text{ nm}$ , hence, the domain structure was optically averaged. The angular dependence of its optical transmission of a cell placed between crossed polarizers is only slightly asymmetric, as seen in Fig. 4(a) (a curve for  $U=0$ ). Here,  $\alpha$  is the angle between the rubbing direction and the polarizer axis, an analyzer being in the crossing position. Under an electric field applied, stripe domains appear

perpendicular to the rubbing direction. The brightness of the neighboring stripes alternates upon field polarity switching. An example is shown in Figs. 3(b),(c): switching of voltage from  $-80$  V to  $+80$  V converts white stripes into black ones and vice versa.

When a sequence of positive and negative pulses of duration  $t_p = 20$  ms separated by 100 ms interval is applied to the cell, the optical response at  $\alpha = 0$  is positive, independent of field polarity: in Fig. 4(a) the transmission at  $U = \pm 100$  V is higher than that at  $U = 0$ . Upon rotation of a microscope table the optical response disappears at a certain critical angle (or “magic point”) about  $\alpha = 20^\circ$ . On further increase in  $\alpha$ , the pulses become negative for both field polarity.

Such a behavior can easily be understood with a very simple model. Imagine, that each domain subsystem has its own chirality, right ( $R$ ) and left ( $L$ ). In the ground state ( $U = 0$ ), the directors of both subsystems are parallel to the rubbing direction. However, when, say, a positive field is applied, the director of  $R$  ( $L$ ) domains rotates clockwise (counterclockwise) by an angle  $\Psi$  ( $-\Psi$ ) dependent on field, and the inverse picture is observed for the negative voltage pulse. Therefore, the directors of the two domain subsystems always rotate in opposite directions and may be considered as two rotating birefringent plates. Then the total intensity of transmitted light is a sum of the intensities transmitted by each domain subsystem

$$\begin{aligned} I &= I_R + I_L = I_0(A/2)\sin^2 2(\alpha - \Psi) + I_0(A/2)\sin^2 2(\alpha + \Psi) \\ &= I_0A(1 - \cos 4\alpha \cos 4\Psi)/2. \end{aligned} \quad (9)$$

Here,  $I_0$  is intensity of light incident onto a cell and polarized along  $\alpha = 0$ , angle  $\Psi$  is taken from the rubbing direction, and  $A$  is the total area of the cell. The total optical transmission of the domain system  $T = I/I_0$  corresponding to Eq. (9) is plotted in Fig. 4(b). The dotted curve ( $\Psi = 0$ ) in Fig. 4(b) corresponds to the curve  $U = 0$  in Fig. 4(a). One can also see that there are two “magic” points at  $\alpha = \pm \pi/8 = 22.5^\circ$ , where the transmission is independent of  $\Psi$ , that is, of applied voltage. From comparison of Figs. 4(a) and 4(b), we can conclude that the field-induced angle of the director rotation is about  $\Psi \approx 18^\circ - 20^\circ$  (this corresponds to the maximum contrast in Figs. 3(b) and 3(c)). Despite the extremely simple model considered, our experimental results shown in Fig. 4(a) are in good agreement with Eq. (9). From this consideration and earlier results [16], it is quite evident that we deal with two almost equal chiral domain subsystems, each being antiferroelectric with either left or right handedness.

### B. AF-F threshold

An example of the hysteresis type curve of the optical transmission  $T_{opt}$  vs external field (polar pulses) is shown in Fig. 5. The steepest growth of  $T_{opt}$  corresponds to the threshold voltage  $U_{th}$  or field  $E_{th} = U_{th}/d$  related to the field-induced AF-F transition, although the latter is not as abrupt as in chiral AFLCs. To find it with good accuracy the signal from the photomultiplier was differentiated with an RC circuit in order to follow a distinct peak at the steepest part of

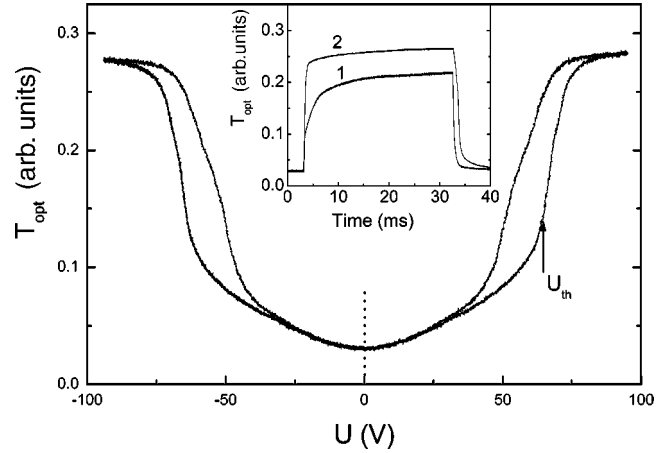


FIG. 5. Hysteresis of the optical transmission on the applied voltage scale ( $U_{th}$  is threshold voltage for AF-F transition). Inset: oscillograms of the electro-optical response at the threshold voltage 70 V (1) and at a voltage  $U = 100$  V exceeding threshold (2). Temperature  $71.4^\circ\text{C}$ .

the  $T_{opt}(U)$  curve. In this way, the whole temperature dependence of the threshold voltage for the field-induced transition from the antiferroelectric to ferroelectric state has been measured, see Fig. 6.

As in a chiral AFLC, the threshold decreases considerably with increasing temperature. With the polarization known from our previous paper [16], it is easy to calculate the interlayer potential from Eq. (4):  $W = 2U_{th}/dP_0$ . We have not used Eq. (7) which predicts 1.5 times higher threshold for the same  $W$  because, in our case, the transition is not as sharp as required by the theory for a first-order field transition and Eq. (7) would overestimate the  $W$  potential. Even with Eq. (4) the value of  $W$  is rather high (6–15 kPa) in comparison with data on chiral AFLC (e.g.,  $W \approx 0.5\text{--}3$  kPa in Ref. [24]). Curve  $W(T)$  shown in Fig. 6 is exponential with relatively small activation energy 0.18 eV (the straight line in coordinates  $\ln W$  vs  $1000/T$  is displayed in the inset to Fig. 6).

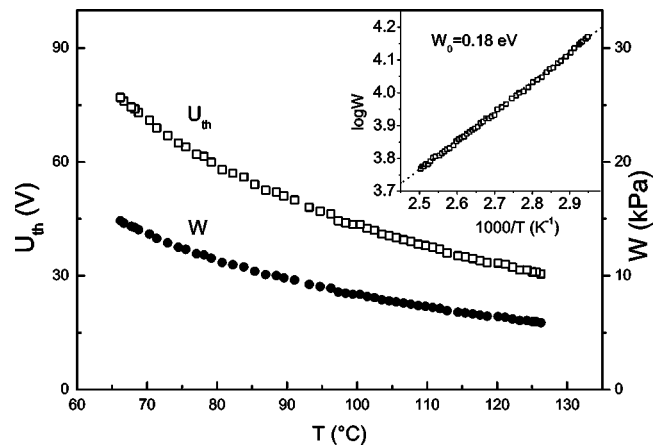


FIG. 6. Temperature dependencies of threshold voltage for the field-induced AF-F transition and calculated interlayer potential  $W$ . Inset: Logarithm of interlayer potential as a function of inverse temperature.

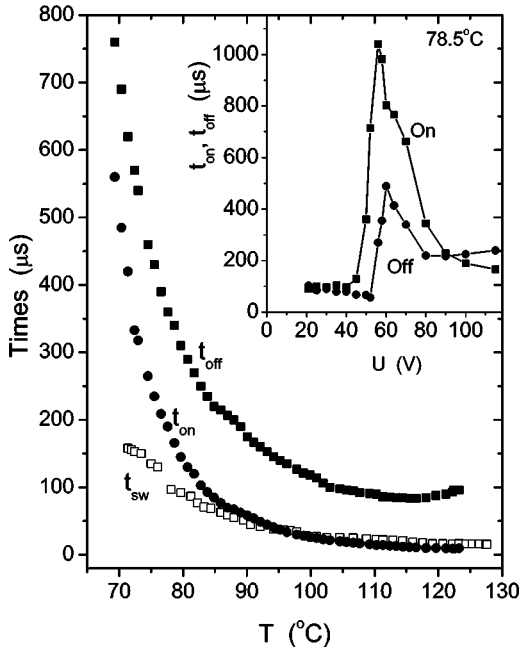


FIG. 7. Temperature dependencies of switching times (1) for the field-induced F-F transition (curve  $t_{sw}$ ). (Polarization was measured with square form voltage  $U=100$  V,  $f=50$  Hz); (2) for the field-induced AF-F transition (curve  $t_{on}$ ). (Electro-optical response was measured with positive and negative pulses  $U=100$  V, duration 20 ms, full period 200 ms); (3) for F-A relaxation (curve  $t_{off}$ ) (same polar pulses). Inset: Field-induced ( $t_{on}$ ) and relaxation ( $t_{off}$ ) times as functions of the applied voltage (polar pulses,  $T=78.5$  °C).

### C. F-F switching

When square form high voltage  $U > U_{th}$  is applied to a cell the polarization and the director in all smectic layers are switched from one field induced F-state to the opposite one. The kinetic curves of the repolarization current show only one peak without any evidence for the ground AF state [15,16]. The switching time  $t_{sw}$  is easily found from the width of the current peak at a half of its height and the result is shown in Fig. 7 for square-wave voltage of  $U=100$  V at frequency 50 Hz. The corresponding viscosity coefficient was calculated from the relationship well known for FLCs [6]

$$\gamma_{\varphi}(F-F) = \frac{P_0(U - U_R)t_{sw}}{1.8d}. \quad (10)$$

Here,  $U_R$  is a part of the applied voltage fallen across the load resistor  $R$  ( $R=2$  kΩ).

The viscosity  $\gamma_{\varphi}(F-F)$  decreases with increasing temperature from 3.8 to 0.2 Pa s and is comparable with the value of about 0.05 Pa s reported for another banana-shaped compound at a higher temperature  $T=135$  °C [18]. The Arrhenius plot shown in Fig. 8 (curve F-F) gives more or less permanent slope 0.74 eV only in the range 70–107 °C. With further increasing  $T$  the slope reduces down to about 0.5 eV.

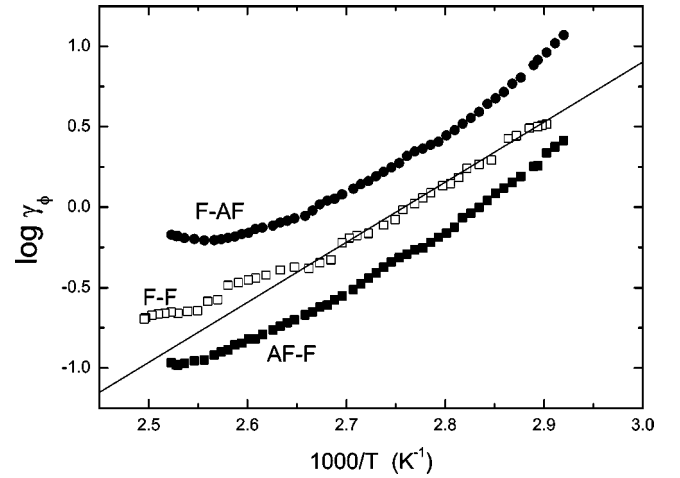


FIG. 8. Arrhenius plots of  $\gamma_{\varphi}$  viscosity calculated for three different switching regimes F-F, A-F, and F-A. Straight line shows activation energy 0.74 eV.

### D. A-F switching and F-A relaxation

These measurements have been done with polar pulses of high duty ratio. First, consider voltage dependencies of the electro-optical response times at a fixed temperature. An example is shown in the inset to Fig. 7. For all of the  $t_{on}(U)$  curves a characteristic maximum is seen at the AF-F transition threshold. It is illustrated by two oscillograms in the inset to Fig. 5. This maximum in  $t_{on}$  may even be used for measuring the threshold voltage  $U_{th}$  but this technique is not as precise as that described above. At voltages  $U > U_{th}$  the inverse switching-on time  $t_{on}$  can be approximated by a straight line in accordance with formulas (4) and (5). Therefore, using

$$\gamma_{\varphi}(AF-F) = \frac{P_0(U - U_{th})t_{on}}{1.8d}, \quad (11)$$

we calculate the viscosity coefficients for the AF-F transition. Coefficient 1.8 relating time  $t_{on}$  of the 10–90 % optical transmission rise time to characteristic time  $\tau_{AF}$  was taken by analogy with FLC [25]. The viscosity coefficients found from voltage dependencies of  $(t_{on})^{-1}(U)$  at several temperatures are consistent with data on viscosity found from  $t_{sw}$  shown in Fig. 7. This result allowed us to measure the temperature dependence of electro-optical rise time  $t_{on}$ , using polar pulse amplitude  $\pm 100$  V, and calculate viscosity  $\gamma_{\varphi}(AF-F)$  with Eq. (11) from  $t_{on}$  and the threshold voltage displayed in Fig. 6. The viscosity found this way varies from 0.6 to 12 Pa s and the corresponding Arrhenius plot is presented in Fig. 8.

Going back to the inset to Fig. 7, we see that voltage dependencies of the relaxation times  $t_{off}$  back to the ground AF state show only weak variations close to the AF-F transition. Therefore, we may use Eq. (6), at least, tentatively in order to find new viscosity  $\gamma_{\varphi}(F-AF)$  from the electro-optical decay time  $t_{off}$  shown in Fig. 7.

$$\gamma_{\varphi}(F-AF) = \frac{2Wt_{off}}{2.3}. \quad (12)$$

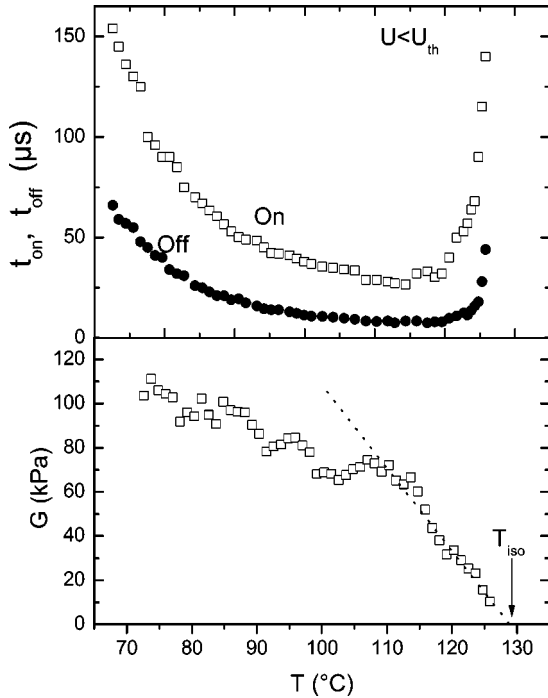


FIG. 9. Top: temperature dependence of electro-optical  $t_{on}$  and  $t_{off}$  times measured with a voltage below the AF-F threshold (polar pulses  $U=23$  V, duration 4 ms, period 80 ms). Bottom: generalized elastic modulus  $G(T)$  calculated from  $t_{off}$  and  $\gamma(F-F)$ . Dotted line shows a slope  $3.6 \times 10^3$  Pa/K.

With increasing temperature viscosity  $\gamma_\varphi(F-AF)$  varies within the range 0.13–3.4 Pa s, its Arrhenius presentation is also shown in Fig. 8.

The general behavior of the Arrhenius plots for F-F, AF-F, and F-AF transitions is similar: in the range of 70–110 °C the slope is approximately same, about 0.75 eV, at higher temperatures it markedly decreases. As to the magnitude of  $\gamma_\varphi$  the data of the three methods are within factor of 3, which is not surprising in view of the simplest approach used (simplified form of the interlayer potential, linearization  $\sin \Phi \rightarrow \Phi$ , assumption of an infinite uniform sample, etc.). For example,  $t_{off}$  times are certainly voltage dependent, even there are small peaks near the threshold quite evident in the inset to Fig. 7. It may point to the importance of second harmonic in the interlayer potential  $J$  [20] or to interaction between not only the neighboring layers but also between more distant layers [12]. A reason for a deviation from the Arrhenius law in the range 110–125 °C is not clear yet.

### E. Dynamic behavior below threshold

Below the AF-F threshold  $E_{th}$ , a pulse electro-optical response is rather weak; the transmission amplitude is proportional to  $E^2$ , as can be seen in Fig. 5. The corresponding on- and off times are voltage independent and always  $t_{on} > t_{off}$ . In Fig. 9 an example is given of temperature dependencies of the rise and decay times measured with polar pulses of 23 V amplitude. In this particular case, measured times ( $t_{on} \approx 30$ –150  $\mu$ s,  $t_{off} \approx 5$ –60  $\mu$ s) are quite short,

therefore, polar pulses with duration 4 ms and period 80 ms were used (even pulses with duration 200  $\mu$ s were tested with the same result).

Let us assume that the director switching at low field is controlled by the same viscosity as at higher field. Then one can estimate an apparent elastic modulus  $G = \gamma/\tau = 2.3\gamma/t_{off}$  from the relaxation times  $t_{off}$ . For calculation of  $G$ , we take  $\gamma(F-F)$  from Fig. 8 and the resulting curve  $G(T)$  is shown at the bottom of Fig. 9.

The attempts to understand this curve in terms of the azimuthal  $\Phi$  distortion seem to have no perspective. On the one hand, modulus  $G$  is too high and has quite different temperature dependence as compared to parameter  $W$  shown in Fig. 6. On the other hand, if one assumes the  $G = Kq^2$  form, where  $K$  is nematiclike modulus and  $q = 2\pi/\Delta$  is wave vector of some inhomogeneity, then the characteristic size of the latter would be too small: with  $K = K_N \sin^2 \vartheta \approx 10^{-11} N$ ,  $\Delta \approx 45$  nm is only one order of magnitude larger than the interlayer distance. The  $G(T)$  behavior reminds, however, that of the soft mode, observed earlier in vicinity of the Sm- $C_A$ –Sm-A transition in chiral AFLCs [10,11].

As well known, at the Sm-A–Sm- $C_A$  transition the soft mode is related to antiphase fluctuations of the molecular tilt angle. Such a tilt is a part of the antiferroelectric order parameter. In our case, there is no Sm-A, and the antiferroelectric order appears simultaneously with the orientational (nematic) and positional (smectic density wave) orders at the same first-order transition. In such a case, fluctuations of different order parameters can coexist. An example is linear electro-optical (“electroclinic”) effect in a chiral nematic phase near the first-order transition to Sm- $C^*$  phase [26,27]. Of course, the fluctuations exist at both sides of the transition although are observed with different techniques. In our case, the curve  $G(T)$  diverges at the  $B_2$ –Iso transition pointing to the existence of antiferroelectric soft-mode fluctuations. From the slope shown by the dotted line in Fig. 9 (bottom), it is possible to estimate an apparent Landau coefficient  $\alpha_{app}$ . A value  $\alpha_{app} = 3.6 \times 10^3$  Pa/K typical of the FLCs [28] is obtained. It is not surprising because the same molecular tilt is involved in both cases.

Since our electro-optical response below  $U_{th}$  is proportional to  $E^2$ , we believe that the high temperature divergence of the curves  $t_{on}$  and  $t_{off}$  is related to the antiferroelectric soft-mode behavior, see Eq. (1), and at low field, we observe a kind of the electroclinic effect. However, this effect is not linear due to symmetry of the AF phase [7] and induced either by term  $\varepsilon_a E^2$  ( $\varepsilon_a$  is dielectric anisotropy unfortunately unknown) or by term  $P_0^2 E^2/4W$  such that in Eq. (8). Probably for this reason on- and off- times are not equal as typical of the FLCs. It should be noted, however, that the soft-mode dynamics is controlled not by azimuthal viscosity  $\gamma_\varphi$  but by tilt viscosity  $\gamma_\vartheta \approx \gamma_\varphi/\sin^2 \Theta \approx 4\gamma_\varphi$ . Therefore, the correct value of  $\alpha_0$  corresponding to our experiment should be somewhat higher than  $10^4$  Pa/K.

### V. SUMMARY

In conclusion, a study of the field-induced optical transmission and polarization switching has been carried out over

the whole temperature range of the antiferroelectric  $B_2$  phase formed by an achiral compound consisting of bent-core shape molecules. The optical texture shows two types of chiral domains. A field-induced director rotation has opposite direction for each set of domains. The interlayer potential  $W$ , which describes the interaction between neighboring anti-clinic smectic layers has been found from the threshold of the transition for the ground antiferroelectric (AF) to field-induced ferroelectric (F) states. The rotational viscosity coefficients  $\gamma_\varphi(AF-F)$  and  $\gamma_\vartheta(F-F)$  have been calculated from the times of the field-induced director switching over azimuthal angle  $\Phi$  between AF-F and F-F states, and viscosity  $\gamma_\varphi(F-AF)$  was calculated from the time of free  $\Phi$  relaxation from F to AF state. All the three coefficients have the same temperature dependence but their magnitude differs by factor 3. The latter is related to oversimplified approximations used for the calculations. The electro-optical re-

sponse was also observed below the AF-F threshold. In this regime, the optical transmission depends on electric field squared. This effect was attributed to the antiferroelectric soft-mode distortion of the amplitude of the molecular tilt angle in the vicinity of the transition from the  $B_2$  phase to the isotropic phase. The corresponding elastic modulus has been found.

#### ACKNOWLEDGMENTS

We thank S. A. Pikin, B. I. Ostrovskii, N. M. Shtykov, and S. P. Palto (Inst. of Crystallography, Moscow) for helpful discussions and F. V. Podgornov (Darmstadt Technical University) for making domain video recording. The work was carried out in the framework of RFBR (Project No. 01-02-16287) and Fondecyt 2000 (Project No. 7000845).

- 
- [1] F. Tournilhac, L.M. Blinov, J. Simon, and S.V. Yablonsky, *Nature (London)* **359**, 621 (1992).
- [2] T. Niori, T. Sekine, J. Watanabe, T. Furukawa, and H. Takezoe, *J. Mater. Chem.* **6**, 1231 (1996).
- [3] E. Soto Bustamante, S.V. Yablonskii, B.I. Ostrovskii, L.A. Beresnev, L.M. Blinov, and W. Haase, *Liq. Cryst.* **21**, 829 (1996).
- [4] W. Weissflog, Ch. Lischka, T. Benne, T. Scharf, G. Pelzl, S. Diele, and H. Kruth, *Proc. SPIE* **3319**, 14 (1997).
- [5] D.M. Walba, E. K orblova, R. Shao, J.E. MacLennan, D.R. Link, and N.A. Clark, *Science* **288**, 2181 (2000).
- [6] S.T. Lagerwall, *Ferroelectric and Antiferroelectric Liquid Crystals* (Wiley-VCH, Weinheim, 1999).
- [7] I. Muševič, R. Blinc, and B. Žekš, *The Physics of Ferroelectric and Antiferroelectric Liquid Crystals* (World Scientific, Singapore, 2000).
- [8] L.M. Blinov, *Liq. Cryst.* **24**, 143 (1998).
- [9] D.R. Link, G. Natale, R. Shao, J.E. MacLennan, N.A. Clark, E. K orblova, and D.M. Walba, *Science* **278**, 1924 (1997).
- [10] K. Hiraoka, H. Takezoe, and A. Fukuda, *Ferroelectrics* **147**, 13 (1993).
- [11] H. Moritake, Y. Uchiyama, K. Myojin, M. Ozaki, and K. Yoshino, *Ferroelectrics* **147**, 53 (1993).
- [12] J.-H. Kim, J.-H. Lee, and S.-D. Lee, *Mol. Cryst. Liq. Cryst. Sci. Technol., Sect. A* **302**, 99 (1997).
- [13] W.K. Robinson, H.F. Gleeson, M. Hird, A.J. Seed, and P. Styring, *Ferroelectrics* **178**, 249 (1996).
- [14] G. Pelzl, S. Diele, and W. Weissflog, *Adv. Math.* **11**, 707 (1999).
- [15] M. Zennoji, Y. Takanishi, K. Ishikawa, J. Thisayukta, J. Watanabe, and H. Takezoe, *Jpn. J. Appl. Phys., Part 1* **39**, 3536 (2000).
- [16] M.I. Barnik, L.M. Blinov, N.M. Shtykov, S.P. Palto, G. Pelzl, and W. Weissflog, *Liq. Cryst.* **29**, 597 (2002).
- [17] A. Jakli, S. Rauch, D. L otzsch, and G. Heppke, *Phys. Rev. E* **57**, 6737 (1998).
- [18] G. Heppke, A. Jakli, S. Rauch, and H. Sawade, *Phys. Rev. E* **60**, 5575 (2000).
- [19] W. Weissflog, Ch. Lischka, S. Diele, G. Pelzl, and I. Wirth, *Mol. Cryst. Liq. Cryst. Sci. Technol., Sect. A* **328**, 101 (1999).
- [20] T. Qian, and P.L. Taylor, *Phys. Rev. E* **60**, 2978 (1999).
- [21] J.F. Li, X.Y. Wang, E. Kangas, P.L. Taylor, C. Rosenblatt, Y. Susuki, and P.E. Cladis, *Phys. Rev. B* **52**, 13 075 (1995).
- [22] E.P. Pozhidaev, M.A. Osipov, V.G. Chigrinov, V.A. Baikalov, L.M. Blinov, and L.A. Beresnev, *Zh. Eksp. Teor. Fiz.* **94**, 125 (1988).
- [23] B. Wen, S. Zhang, S.S. Keast, M.E. Neubert, P.L. Taylor, and C. Rosenblatt, *Phys. Rev. E* **62**, 8152 (2000).
- [24] M. Kimura, D. Kang, and C. Rosenblatt, *Phys. Rev. E* **60**, 1867 (1999).
- [25] J.-Z. Xue, M.A. Handschy, and N.A. Clark, *Ferroelectrics* **73**, 305 (1987).
- [26] L. Komitov, S.T. Lagerwall, B. Stebler, G. Anderson, and K. Flatischler, *Ferroelectrics* **114**, 167 (1991).
- [27] L.M. Blinov, L.A. Beresnev, and W. Haase, *Ferroelectrics* **181**, 211 (1996).
- [28] L.M. Blinov, L.A. Beresnev, and W. Haase, *Ferroelectrics* **174**, 221 (1995).